JOURNAL OF MATERIALS SCIENCE: MATERIALS IN MEDICINE 7 (1996) 479–488

Substitution of natural coral by cortical bone and bone marrow in the rat femur

Part II *SEM, TEM, and* in situ *hybridization*

C. MÜLLER-MAI, C. VOIGT, S. R. DE ALMEIDA REIS*,
H. HERBST*, U. M. GROSS*
*Department of Traumatology and Reconstructive Surgery and *Institute of Pathology, Klinikum Benjamin Franklin, Freie Universität Berlin, Hindenburgdamm 30, D 12200 Berlin, Germany*

Natural coral consisting of calciumcarbonate ($CaCO_3$) in the crystal form of aragonite was investigated after implantation into the cortex and marrow cavity of rat femur at 7, 14, 21, and 28 days by means of scanning and transmission electron microscopy (SEM and TEM) as well as *in situ* hybridization (ISH) in order to better understand its mechanism of bone bonding, which is somewhat different to that of other slowly degradable bioactive materials, e.g. hydroxyapatite or glass ceramics. Bone bonding was shown to be closely coupled with implant degradation. Degradation by dissolution started as early as the insertion of the implant leading to a pronounced surface rugosity. Additionally, at later stages, degradation by multi-nucleated osteoclast like cells was enhanced. Bone bonding was mediated by flat cells settling in groups on the implant surface. These cells produced mineralizing globules and collagen that anchored directly to the implant surface, i.e. on the tips of the surface rugosity and inside the pores. Through ISH the cells were shown to produce procollagen α1(I) transcripts. The calcification at the interface was enhanced by matrix vesicles similar to woven bone formation. Therefore, the calcification on the implant surface resembled woven bone formation and no distinct afibrillar intervening layer resembling a cement-line, as in other bioactive implants or as in bone–bone interfaces, e.g. in lamellar bone was observed in bone bonding areas. The mineralization in deeper micropores which did not include direct cell activity depended on other processes, e.g. dissolution and reprecipitation.

1. Introduction

Coralline implants of the Porites species have been used as bone implant materials since 1977 [1]. The skeleton of such calcium carbonate implants of the crystal type aragonite was first prepared by hydrothermal conversion of skeletal calcium carbonate into hydroxyapatite by treatment in a fluid medium of biammoniumhydrogenphosphate ($(NH_4)_2HPO_4$) and H_2O at 300 °C and high pressure, since it was thought that the implantation of hydroxyapatite (HA) would be closer to bone mineral than natural coral calcium carbonate ($CaCO_3$) [2]. In later experiments the skeletal $CaCO_3$ was deproteinized by treatment with sodium hypochlorite yielding a composition of 99% $CaCO_3$ and 1% amino acids [3]. Later experiments demonstrated that the composition was somewhat different (see Materials and methods). The surfaces of the interconnecting macropores of calcium carbonate provide a framework for tissue growth since there is space for blood vessels in the centre of the pores. Therefore, the coralline material can be used as a scaffold by the system bone forming and resorbing cells and can be remodelled over a long period of time [3, 4]. The porites species possess interconnecting pores of up to 200 μm in diameter and a mean pore diameter of 154 ± 25 μm. The mean pore volume was measured to be 43.5 ± 2% [5]. The deposition and resorption of these implants have been described in several papers at a light microscopical level [3, 4, 6]. It was shown that coralline implants seem to be replaced earlier in trabecular versus cortical bone defects [3]. The degradation rate of this coral seemed to be higher than that of coral being transformed into hydroxyapatite. Degradation was dependent on the pore size range and the total pore volume. The larger the pores, the faster the resorption, and the faster the development of new bone [4]. As compared to porous hydroxyapatite the tissue healing was faster around β-tricalciumphosphate or natural coral [6]. Additionally, a recent investigation showed that the resorption of natural coral implants was faster in contact with bone marrow as compared to cortical bone [7].

With regard to these investigations, not much is known about the events occurring at the interface leading to resorption or to bone bonding. The role of

0957–4530

cells elaborating extracellular matrix and establishing bone bonding seems to be especially important. The role of osteoclasts, macrophages or soft tissue cells in the process of degradation is not clear and the chemical dissolution of the coralline substance is not yet clearly separated from the activity of resorbing cells. Recently, it has been demonstrated that differences occur in the ultrastructure of bone bonding interfaces of glass ceramics, hydroxyapatite and $CaCO_3$. Glass ceramics bond via an afibrillar intervening layer, representing in this case a cement-line-like interface between the implant and the bone, similar to that observed in lamellar bone between two osteons. On the other hand, $CaCO_3$ and β-tricalciumphosphate implants did not show this cement-line-like structure in bone bonding interfaces. Hydroxyapatite was shown to develop both interface types [8, 9]. The mechanisms of different morphological developments are not yet clear. A previous investigation could not maintain the $CaCO_3$ crystals after preparation for TEM [10]. Therefore, since no intact interfaces could be maintained, no evidence could be found for the bone bonding mechanism including the development of the afibrillar intervening layer between implant and bone. As indicated by some publications, the production of collagen seemed to be involved in the bonding process in highly degradable interfaces showing bone bonding interfaces without the afibrillar intervening layer [9, 11, 12]. Therefore, special emphasis was put on the development of collagen on the $CaCO_3$ surface. Additionally, for the first time to the authors knowledge, *in situ* hybridization (ISH) was adapted to implants containing bone using a procollagen α1(I) probe to stain collagen producing cells, although it is known that the production of this collagen is not specific to osteoblasts and that the intracellular assembly is not equated with secretion into the extracellular matrix. Evidence for collagen secretion into the extracellular matrix can be given by morphological methods, such as scanning and transmission electron microscopy (SEM, TEM).

The present investigation aims to further clarify the events occurring in the bone–$CaCO_3$ interface with special attention to the development of bone bonding and degradation. In order to better understand the mechanisms of calcium carbonate degradation by dissolution as well as by cellular resorption, and bone deposition, animal experiments were performed using quantitative histology, the report of which is presented in Part I [7], and TEM and SEM as well as ISH, contained in the present investigation (Part II). Special emphasis was placed on the development of bone bonding since differences in the ultrastructure of bone bonding interfaces of different bonding materials have been observed [8–15]. Since up to now no intact interfaces could be produced for TEM evaluation, another aim was the development of a method to maintain intact tissue–$CaCO_3$ interfaces. Additionally, ISH was adapted to implant containing tissue based on a method published previously [16] to further clarify the role of cells during the bone bonding process.

2. Materials and methods

The natural coral implants (Biocoral^R) were deproteinized cylinders from the species Porites with a diameter of 1.5 mm and length 6 mm. They were sterilized by gamma irradiation and contained more than 97% calcium carbonate in the form of aragonite, less than 1% amino acids (aspartamic acid 0.013%, glutamic acid 0.011%, glycine 0.01% and others in lower quantities), and >1% trace elements (<1% Na, 0.5 to 0.9% Sr, 0.05 to 0.2% Mg, 0.05 to 0.1% F, <0.05% P, <0.03% K and trace elements such as Cu, Zn, Fe, Pb, Mn, Ni, Cr, and Co in much lower amounts) [17]. The macropores interconnected and occupied less than half of the implant volume.

Adult male Sprague-Dawley rats with a body weight at the beginning of the experiment of between 450 and 650 g were housed in wire cages and given a hard pellet diet Altromin standard (Lage, Lippe, Germany) and tap water *ad libitum*. Under general anaesthesia, the femur was exposed and a hole with a diameter of 1.5 mm was drilled midshaft and the implant cylinder inserted. The wound was closed in layers with sutures and the animals given protective treatment with gentamycin 20 mg and 0.5 ml Belapharm Antiphlogisticum 30%. At 7, 14, 21 and 28 postoperative days, three specimens were collected and prepared for SEM and TEM as described [8]. The first TEM sections prepared were stained according to a standardized procedure using uranyl acetate and lead citrate. This led to a total loss of the $CaCO_3$ implant in the section. Therefore, the following sections were only postfixed in OsO_4 1% in cacodylate buffer pH 7.2 at 4 °C overnight. No additional staining was performed. This procedure led to intact interfaces with the disadvantage that non-bonding interfaces could not be evaluated due to low staining contrast of the organic moiety. Therefore, both procedures were applied. One implant was investigated prior to implantation by SEM and one by TEM thus yielding a total of 14 implants for EM. Additionally, 12 implants were used for *in situ* hybridization, three being harvested at 7, 14, 21, and 28 days after insertion.

For ISH, implants containing femur segments were cut into three smaller pieces in a sagittal plane, i.e. the implant was cut perpendicularly to its long axis, and then fixed for 24 h at 4 °C in 4% paraformaldehyde in phosphate buffered saline (PBS), pH 7.0, and afterwards shortly rinsed in pure buffer at pH 7.0. The decalcification of the implant-containing pieces was performed at 4 °C in ethylenediaminetetraacidic acid (EDTA) 10% at pH 7.5 for 7 days on a shaker. With this procedure the implant material totally dissolved. Afterwards the former implant-containing bone was immersed in graded ethanols (70%, 80%, 96%, and absolute ethanol), acetone and xylol. Then, the implants were embedded in paraffin wax (Histosec^R, Merck, Darmstadt, Germany). Sections 4 μm thick were cut with a microtome. The sections were put on aminopropyltriethoxysilane-covered, glutaraldehyde-activated glass slides, dried overnight at 37 °C, and stored at room temperature until ISH was carried out. The trabecular bone from human femoral heads served as a positive control.

2.1. *In situ* hybridization

To generate digoxygenin-labelled RNA probes a 1,3 kb Pst I fragment of rat procollagen α1(I) cDNA [18] was subcloned into the run-off transcription vector pGEM1 which was linearized appropriately and used for *in vitro* transcription with SP6 or T7 polymerases and digoxygenin-labelled UTP (Böhringer, Mannheim, Germany) to obtain antisense and sense (control) transcripts, respectively [19, 20].

The hybridization procedure was identical to the method described earlier except that the amount of the probe was different (0.5 ml of mixture containing 250 µl formamide, 218 µl Depc-H_2O, 32 µl probe RNA at a concentration of 5 ng/µl). Afterwards, the specimens were washed as described [19]. Digoxygenin was then detected using a monoclonal antibody recognizing digoxygenin Fab fragment according to a standardized method [21]. Stained parts of the tissue appeared bright red. The counterstaining was performed by using haemalaum for 1 min. The specimens were embedded in glycerol jelly at 50 °C.

3. Results

3.1. Implants prior to implantation

The SEM overview showed the typical structure of the implants with interconnecting macropores in the range of 150 µm (Fig. 1). At higher magnifications two different surfaces of the natural coral skeleton were detected (Fig. 2). First, there was the surface of the coral which was rather smooth (Fig. 3). At high magnifications tiny tips of less than 1 µm height, probably the tips of individual crystals, were observed covering one part of this area, creating some kind of surface rugosity. Other crystals reached the surface in an oblique direction leading to a less rough structure. In these areas globular elevations of 5 µm in diameter were detected (Fig. 2) occasionally in circumscribed areas. These surfaces represented the original inner surface of the natural coral. Secondly, there were fracture or sawing planes probably existing due to the mode of production showing the individual coral plates in their longitudinal axis. The plates were arranged mainly perpendicular or oblique to the surface and had a length of about 10 µm (Fig. 2). Between individual plates and crystals a microporosity containing some amorphous, probably organic, material was detected. The density of the surface structure was higher at the original inner surfaces than at the fractured surfaces. In TEM the individual plates and crystals observed in SEM were composed of groups of parallel aligned smaller crystallites. These crystallites were probably of plate-like or cylindrical structure (Fig. 4) and were cut in a longitudinal or transverse direction providing in both cases a maximal length of about 2 µm. The maximal width was 1 µm in the case of plate-like crystallites and 0.2 µm in the case of cylindrical crystallites. The cylindrical crystallites might represent the third dimension of the other crystallite type.

3.2. SEM after implantation

At 7 days, using SEM at lower magnifications, the tissue seemed to grow from the cortical area towards the marrow cavity. Larger tissue complexes were already developed interdigitating with the porosity of the implants. At higher magnifications many cells were detected settling on the implant surface. These

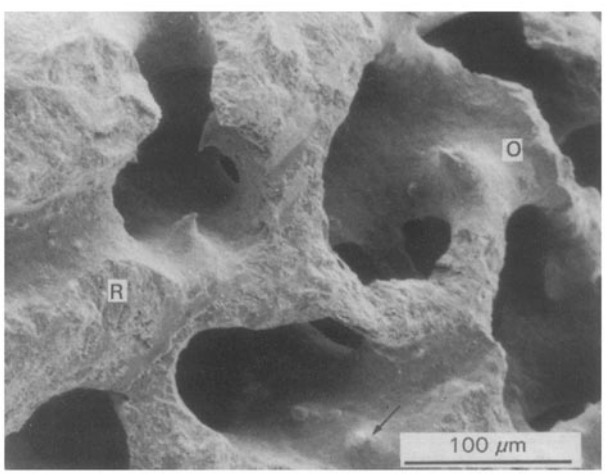

Figure 1 Macropores of coral Porites of size around 150 µm prior to implantation with smooth original surface (O) and fractured rough surface (R). Occasionally hump-like structures (arrow) (SEM).

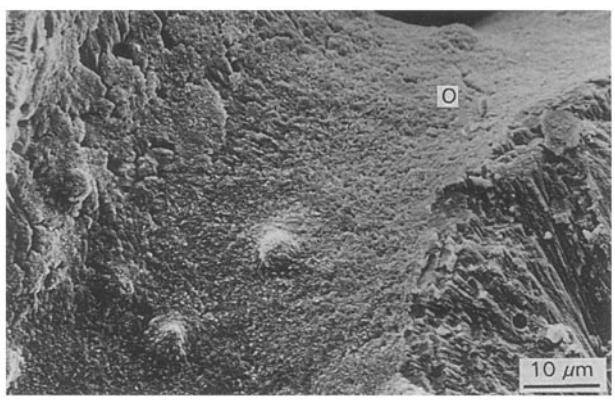

Figure 2 Smooth original surface (O) and fractured rough surface prior to insertion with hump like structures of about 5 µm in diameter (SEM).

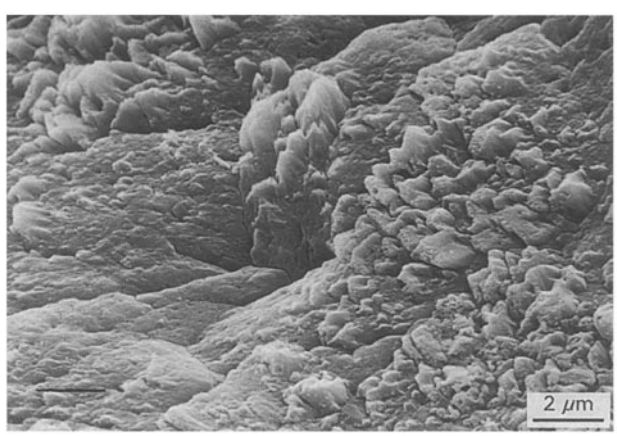

Figure 3 Smooth original surface of the coral with tips on the right side and oblique appearing crystals at left prior to implantation (SEM).

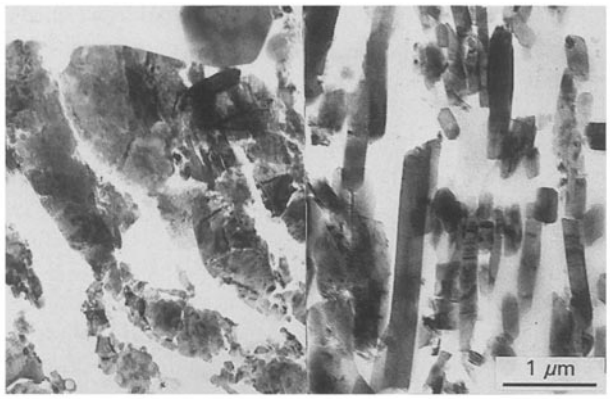

Figure 4 Cross-section of the coralline implant material prior to implantation with both crystal moieties, i.e. plate-like structures on the left side and cylindrical crystals on the right side (TEM, unstained).

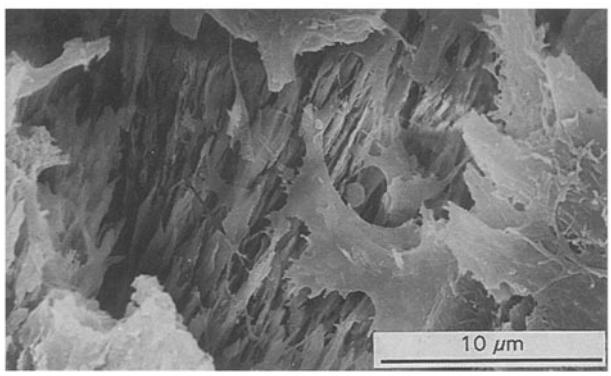

Figure 5 Surface structure of the coral after partial degradation with tips of crystals and gaps. Part of a cell with processes between the tips (arrow) (SEM).

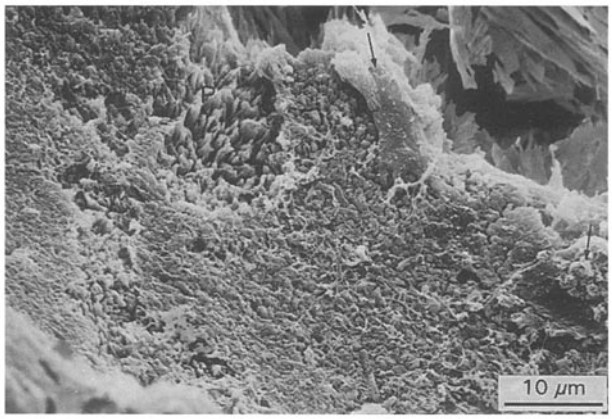

Figure 6 Cells on the surface of the natural coral implant (arrows). Pit (P) and track-like change of the surface structure (SEM).

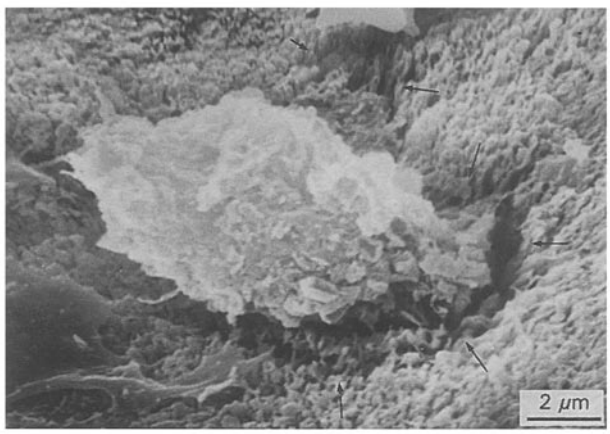

Figure 7 Roundish cell on the surface of a coralline implant settling in a newly created pit (arrows) (SEM).

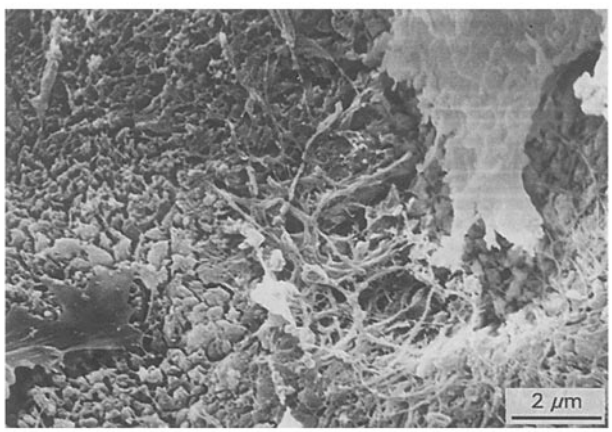

Figure 8 Two cellular processes on left and right side of the coral surface with a pit. Pit already filled with deposited fibrillar material probably produced by the cell on the right side (SEM).

cells were roundish, spindle-like, or rather polygonal and flat and occurred in groups. Some areas of the surface remained unchanged. Other areas of the implant surface had changed significantly. These parts of the surface showed a higher rugosity as compared to the situation prior to implantation, obviously due to loss of substance. Thus, these circumscribed areas of up to 40 µm in diameter showed tips of individual crystals with gaps in between (Fig. 5). Additionally, pits of about 10 µm in diameter and depressions with a track-like morphology were found (Fig. 6). In pits as well as in other areas with changed surface morphology there was a much more pronounced rugosity with some degree of microporosity between crystals. Single roundish cells of about 10 µm in diameter were in contact to these pits (Fig. 7). In some areas flat polygonal cells were observed in close relation to lacunae of the implant surface. These cells deposited fibrillar material into the pores (Fig. 8). Close to groups of polygonal flat cells tiny globular structures and fibrillar structures were deposited between the tips of the implant crystals (Fig. 9). These structures produced a thin film on the implant surface (Fig. 10). Fibres occurred with as well as without globular structures. Some globular structures were in contact with cellular processes. Between the cells of one group such deposits of material were not common.

At 14 days the situation was comparable except that there was much more tissue adhering to the implant surface after fracture, than at 7 days. Therefore, it was much more difficult to detect intact tissue–implant interfaces. Most of the uncovered implant surfaces showed an accentuated rugosity. Between needle-like tips of the $CaCO_3$ crystals there was a considerable porosity. Cellular processes attached directly to single tips. In fracture planes of the interface a fine granular

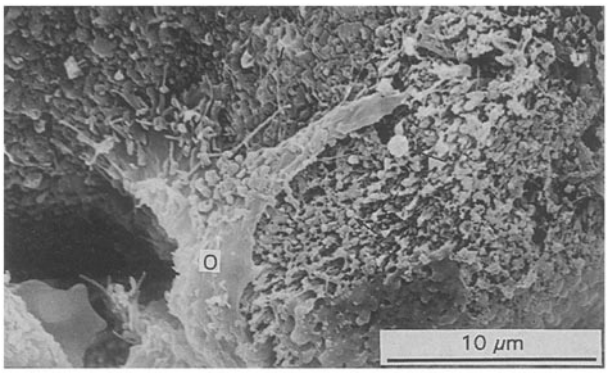

Figure 9 Deposition of thin fibrilles (short arrows) and globular structures (long arrows) between tips of the implant surface by a cell of the osteoblastic lineage (O). Production occurs on roughened surface of the coral (SEM).

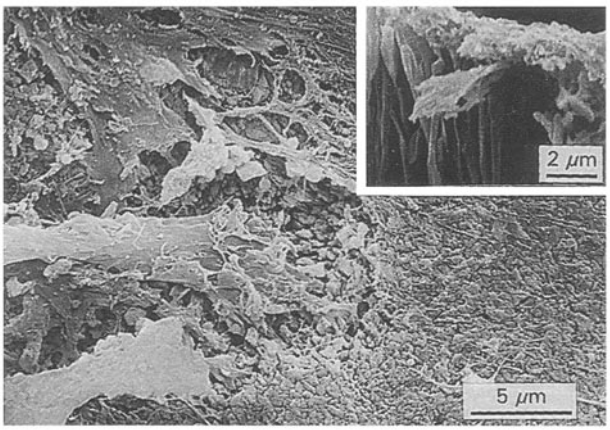

Figure 10 Later stage of production as shown in Fig. 9. A group of osteoblastic cells on the left of the implant surface moving to the left. At right dense film mainly composed of fibres and some globular structures (SEM). Inset: fracture plane of a film covering the implant crystals (SEM).

material was detected in micropores under cells (Fig. 11).

At 21 and 28 days, most of the implant surface was covered with tissue including mineralized bone or cells arranged in a layer. The pores of the natural coral implants were almost completely filled with tissue including an amorphous, mineralized substance. Towards the tissue side this amorphous material was in continuity with mineralized bone, which was recognizable by its typical morphology in fracture planes (Fig. 12). Some fracture planes of the coral were observed in contact with adhering tissue. The porosity disappeared close to the interface due to the amorphous material which had been deposited in the pores. In lower magnification the crystal cluster size decreased from the implant centre towards the surface (Fig. 13).

3.3. TEM after implantation

At 7 days the interface was dominated by cells, generally of two types, in contact with the natural coral. There were electron-lucent, spindle-like cells containing a lot of rough endoplasmic reticulum. Between them, roundish cells of darker appearance were observed containing a lobed nucleus and many mitochondria. The first cells resembled fibroblasts and

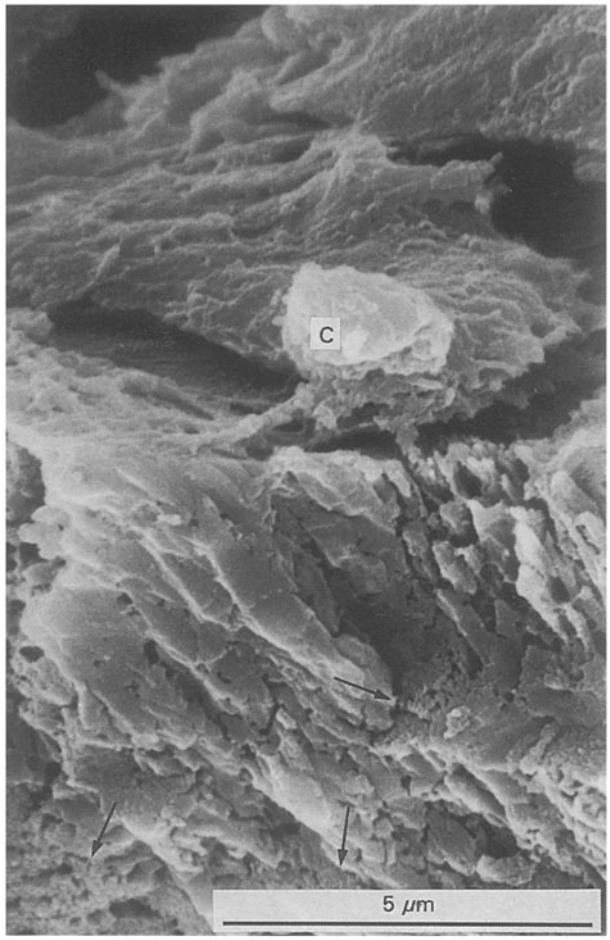

Figure 11 Coral pores mainly filled with amorphous material (arrows) under a cell (C) (SEM, fracture plane).

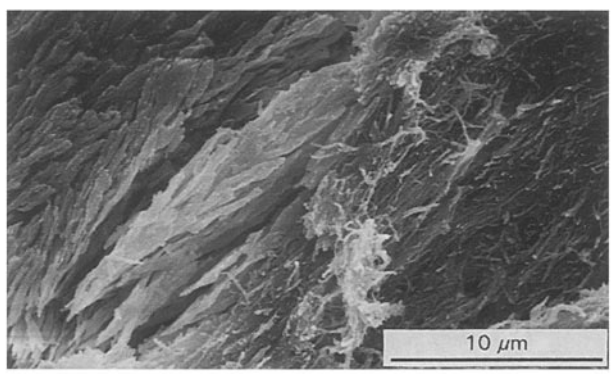

Figure 12 Crystal clusters of the natural coral with microporosity on the left side, bonding to mineralized bone on the right side. Fracture plane of an interface (SEM).

the latter type macrophages. Between these cells lay remnants of cells which had died. Cell detritus was observed within the outer implant pores (Fig. 14). Both types of cellular processes were attached to tips of implant crystals or interdigitated with the porosity. Complexes of implant material lost contact with the surface and were found in the extracellular matrix (ECM) between cells. Some small areas were seen which had already developed bone bonding. The mineralized tissue showed intimate interdigitation with the porosity of the implant and was found within the pores. There was no afibrillar intervening layer between bone and implant. The crossbanding of

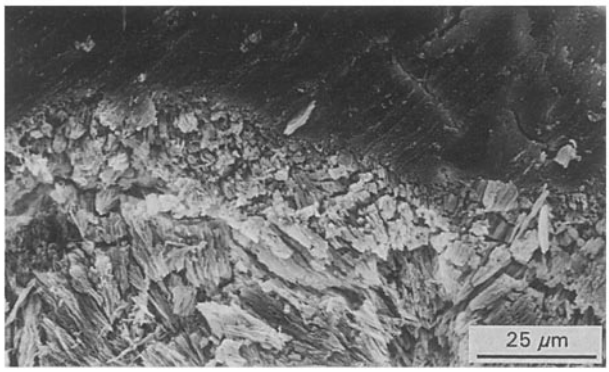

Figure 13 Coral crystal clusters of decreasing size from the centre towards the surface. Bone bonding area, bone in upper part. Sawed section (SEM).

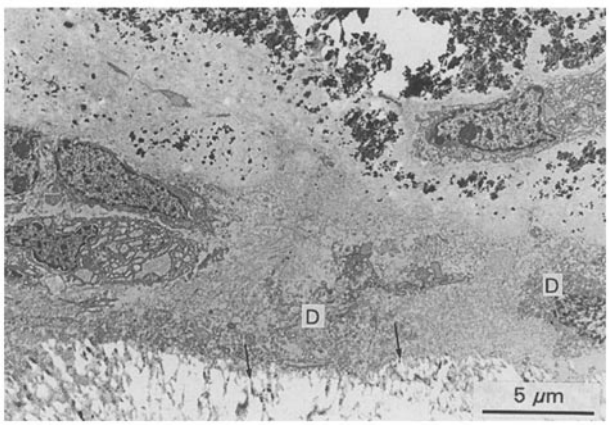

Figure 14 Mineralizing interface with degenerating cells (D) and productive cells in the interface. Cell detritus (arrows) in the pores of the coral (white). Loss of the implant material due to the staining procedure with uranyl acetate and lead citrate (TEM).

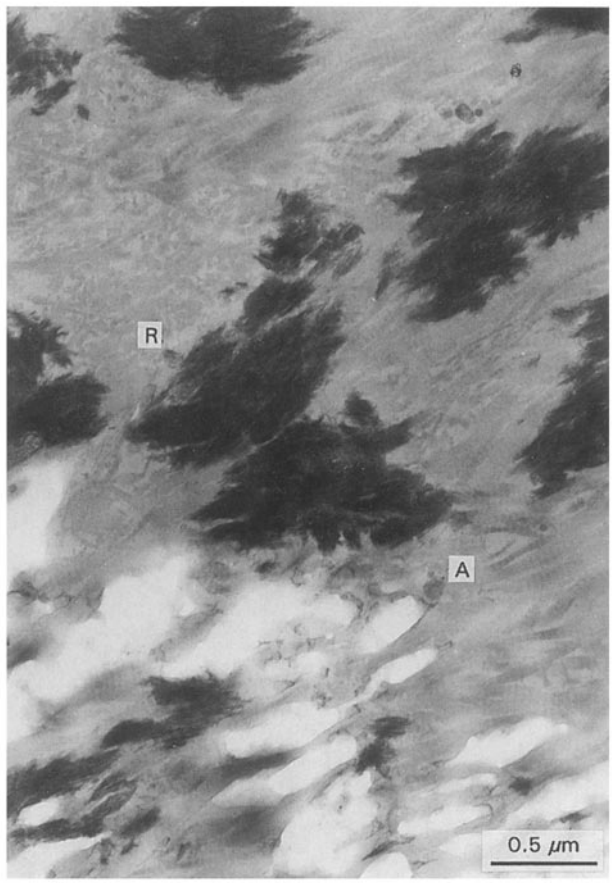

Figure 15 Higher magnification of a mineralizing interface with collagen rich ECM containing matrix vesicles of amorphous (A) and ruptured (R) type as well as calcospheritic structures. Collagen in the pores of the coral (white). Loss of the implant material due to the staining procedure with uranyl acetate and lead citrate (TEM).

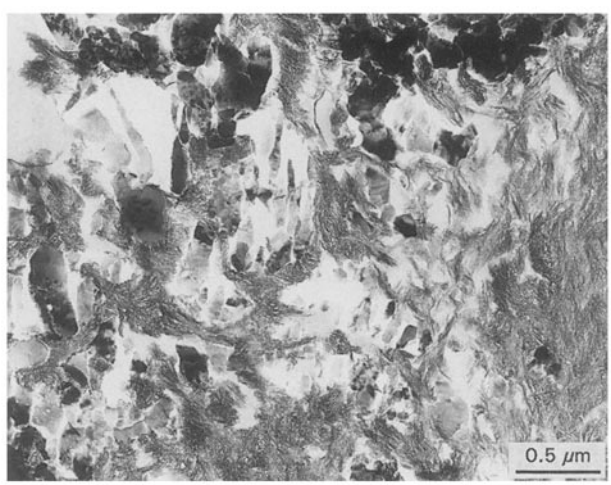

Figure 16 Mineralized interface, mineral proceeding into the pores. No afibrillar intervening layer. Implant particles in the mineralized bone. No staining, OsO_4 fixation (TEM).

collagen fibres, sometimes seen within the mineralized substance, reached the implant surface.

At 14 days bone bonding and non-bonding interfaces were observed. At non-bonding interfaces cells were mainly in contact with the implant surface. Besides the productive cells described at 7 days, multinucleated giant cells were seen with a ruffled border like structure underneath their cell membrane in contact with the implant surface. The filopodia of the ruffled border like structure were interdigitated with individual crystals of the implant. Close to these resorbing cells productive cells were found producing collagen fibres which were inserted on single implant crystals or proceeded into the implant pores. At high magnifications, the collagen-rich ECM contained matrix vesicles at the interface in contact with mineralized bone (Fig. 15). Vesicles were found in close contact to the interface. In such areas there were also so-called calcifying globules in the ECM. The globules confluenced in some areas producing calcifying fronts. The mineralized tissue extended into the implant porosity (Fig. 16). Directly at the interface the crystal size decreased significantly. Small granular particles were detected between cellular membranes and the implant material (Fig. 17).

At 21 and 28 days, the situation was similar to that at 14 days. In non-bonding interfaces many multinuclear giant cells were detected. There were many particles which had lost contact with the surface. Some of these particles were freely floating in the ECM, and others were phagocytosed by cells. The particle size seemed to decrease from the centre towards the surface of the material (Fig. 18). Bone bonding areas showed no afibrillar intervening cement-line like layer. The mineralization proceeded deep into the porosity (Fig. 19). The amount of bone in contact with

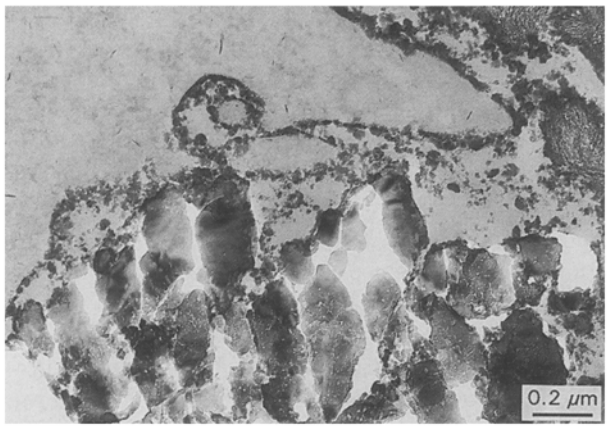

Figure 17 Particulate degradation at the implant surface in the vicinity of a cell (on the left side). Mineral on the right side. No staining, OsO_4 fixation (TEM).

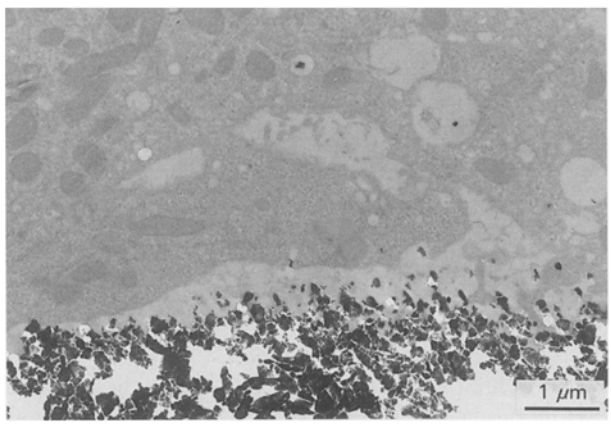

Figure 18 Part of a multi-nucleated giant cell with many mitochondria and extracellular indentations. Some implant material surrounded by membranal parts. Particulate degradation of the implant and crystal size decreasing towards the implant surface. No staining, OsO_4 fixation (TEM).

the natural coral was higher in the TEM sections than at the former time intervals.

3.4. ISH after implantation

Because of the cutting process the implant-containing material had to be decalcified. Therefore, the implant material was lost totally. Instead of the natural coral implants empty spaces were observed. The pores were filled with tissue. At 7 days most of the tissue within the pores in the periphery of the implant cylinders was young forming bone. In the centre of the implants soft tissue was in the pores. The digoxygenin stain provided an intense bright red colour of procollagen α1(I) mRNA containing cells. Such a positive signal was demonstrated by the presence of osteoblasts in lacunae, found in the newly formed primary bone within the drill hole. A similar signal was observed in the cells in the young trabeculae within the implant pores whereas old lamellar bone remained negative (Fig. 20). In the soft tissue only single cells in the periosteum showed a weak signal, mainly on the periosteal side of the femur. The old bone cells surrounding the drill hole were negative. Occasionally, single osteoblast seams showed a positive reaction indicating procollagen synthesis. At 14 to 28 days the situation was comparable, except that the amount of young woven bone in the implant porosity increased with time, and cells lying in lacunae, probably osteocytes, tended to remain negative, whereas cells of osteoblast seams still showed the intense positive reaction. In the centre of the implants there were still some negative organization tissue and some procollagen forming spindly cells which were interpreted as fibroblasts since in their

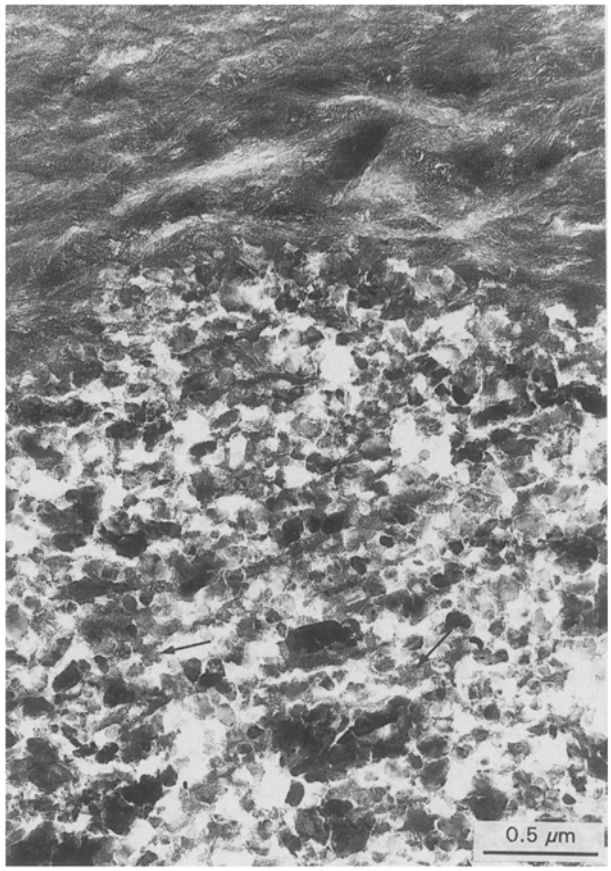

Figure 19 Mineralized bone bonding interface without an afibrillar intervening cement-line like layer. Mineralization in the pores up to more than 5 μm towards the implant centre (arrows) (TEM, OsO_4 fixation without additional staining).

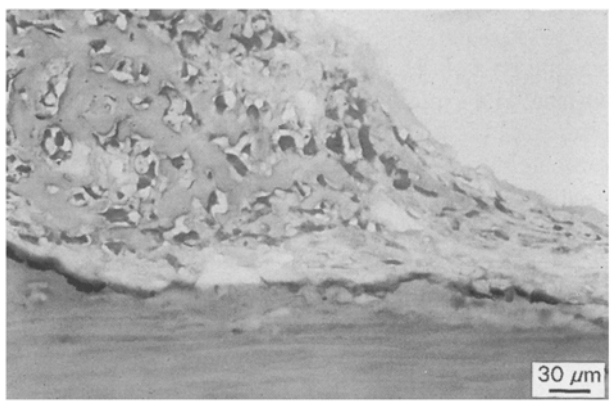

Figure 20 Cross-cut section of a rat femur after visualization of procollagen alpha 1(I) by ISH using digoxygenin staining at 7 days after implantation. Old lamellar bone of the drill hole without staining (bottom). Osteoblasts at the surface of the old bone and young forming bone with intensely stained cells (to the left). Empty space at the upper right corner due to dissolution of coral by EDTA immersion. (Light micrograph).

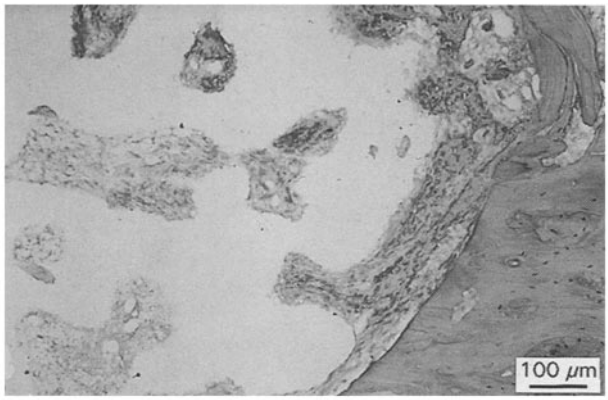

Figure 21 Light micrograph of a cross-section at 14 days after implantation after ISH. Old lamellar bone of the drill hole without staining (on the right side), osteoblasts on the old bone with intense red reaction. Young forming bone within the pores of the implant with many intensely stained cells. Empty space due to dissolution of the coral by EDTA immersion (Light micrograph).

surroundings the extracellular matrix did not correspond with bone ECM (Fig. 21).

4. Discussion

The present investigation proved that the development of bone bonding in the case of a highly degradable implant material such as $CaCO_3$ in the form of aragonite occurs in a different manner as compared to slowly degradable bioactive materials, e.g. glass ceramics and HA, since no afibrillar intervening layer resembling a cement line known from lamellar bone could be discriminated. Generally, two basic mechanisms, both contributing to bone bonding, have been described. First, Kokubo *et al.* proposed a mechanism leading to a carbonated apatite layer on the implant surface when immersed in a simulated body fluid *in vitro* [22]. This process depends on dissolution and reprecipitation since cells were not involved in this model. On the other hand, Davies *et al.* proposed the formation of a similar layer by a cell-mediated process. These data were obtained by using an osteoblastic cell culture system and titanium substrate [23]. A similar layer was observed *in vivo* many years ago [24]. In bioactive implants, e.g. glass ceramics *in vivo*, this layer was a constant phenomenon [9, 13, 15]. Some authors observed a layer on HA in bone bonding interfaces, whereas it did not appear in cases of bone marrow contact [15]. Other authors even detected differences in bonding interfaces, i.e. in some bone bonding areas the layer was not detected [8, 11, 12]. These areas of direct bone–implant contact without intervening layer were comparable to bone bonding interfaces observed in highly degradable $CaCO_3$ implants. Therefore, different variables must be operative in the establishment of bone bonding interfaces without the afibrillar intervening layer. The morphology of bone bonding interfaces seems to depend at least to some extent on the surface reactivity of the implant.

In the case of $CaCO_3$, as early as the implant was inserted, dissolution of the coralline surface started leading to some kind of rugosity of the implant surface. This was clearly demonstrated by comparison of non-implanted and implanted surfaces using SEM. The rough surface structure became colonized by cells, e.g. fibroblasts, pre-osteoblasts or osteoblasts. It has already been shown that natural coral is a very suitable material for cell attachment [25]. The cells seemed to settle on cellular processes which were anchored on the tips of the implant material. No clear evidence was found that a direct deposition of mineralized substances occurred into the gaps deeper than approximately 1 µm. On the other hand, the cells were in close relation to globular structures at the interface which were shown using TEM to be so-called calcospheritic structures. In a similar manner, collagen was directly deposited on the implant surface by the same cells (Figs 8, 9) sometimes proceeding into the gaps up to 1 µm depth. A similar collagen attachment directly at the implant surface has been described for tricalciumphosphate in the form of β-whitlockite which is also highly degradable [26]. This is in contrast to the current concept of bone bonding which acts on more stable surfaces, i.e. pre-existent bone as well as slower degradable materials such as $CaCO_3$. In this case globular accretions are produced by flattened cells which later form a continuous layer on the pre-existent surface. This layer then links up the pre-existent surface and the newly formed collagen-containing bone [27, 28]. Due to the very high reactivity of the implant material used here, a continuous layer of globular accretions could not be established.

Evidence for the collagenous nature of the matrix surrounding osteoblastic cells was found through the ISH method showing osteoblasts to synthesize procollagen α1(I) transcripts. The collagenous matrix contained matrix vesicles and cellular detritus which were shown to act in a comparable manner to matrix vesicles in inducing calcification in a yet non-calcified matrix [13]. The confluence of such calcospheritic structures led to the establishment of calcified fronts similar to woven bone production. Since collagen was deposited directly on the implant surface the cement-line like structure, the so-called amorphous afibrillar intervening layer, could not be distinguished. Therefore, the high degradation rate and rough surface structure of the implants after implantation apparently impede the production of a continuous afibrillar layer. This is distinguishable as a distinct structure and allows for early collagen insertion not only to newly formed globular accretions but also to the tips of the implant surface. Therefore, woven bone formation starts morphologically on the implant surface. Similar results were gained using $CaCO_3$ calcite implants which were also bonded directly to bone. Thin film X-ray diffraction analysis and Fourier transform infrared reflection spectroscopy did not show an intervening layer [29]. Other highly degradable materials, e.g. β-tricalciumphosphate (β-TCP) implants, also bonded without an afibrillar intervening layer [9, 15]. The bonding was explained in this case by mechanical interlocking due to the rough surface structure of the implants. HA/β-TCP composites involved both interface types in bone bonding interfaces [11]. The establishment of the bonding was explained by a process involving epitaxy, dissolution and reprecipitation, and

active secretion of an afibrillar calcified matrix by osteoblast-like cells linking the implant surface and the new collagen containing bone. This explanation is in accordance with previous results from HA implant research. In some interface areas degradation of the surface was observed leading to a rough surface structure. In these areas collagen attachment was observed [8]. If such an interface mineralizes later, the distinct structure known as the afibrillar intervening layer cannot be observed. On the other hand, on a more stable, smooth surface where degradation does not occur, the afibrillar intervening layer becomes more important as a bone–matrix implant interface in a comparable manner to the interface between two lamellae in lamellar bone deposition. The thickness of such layers varies between less than 1 μm (bone–HA interface), which has been reported in the literature [27], up to about 5 μm (lamellar bone interfaces), which is a historical standard.

If there is a similar material to the afibrillar intervening layer in the implants investigated, this is probably represented by the amorphous material observed within deeper micropores, although this material can obviously not have been produced by cells. It was shown in an earlier study [30] that proteins, e.g. osteopontin and osteocalcin, which both have a high affinity to Ca ions, were adsorbed onto the implant surface as well as into the implant pores. These proteins might have helped to create a favourable situation for Ca/P precipitation. In the case of the present implants, Ca might come from the implant liberated by dissolution and resorption as well as from the body fluids, whereas the P source must be the biologic environment. Thus, the precipitation in the pores is different from the mineralization at the implant surface including outer pores up to a depth of about 1 μm. This assumption is supported by a recent study [31]. The authors observed the formation of a carbonated Ca/P-rich layer on $CaCO_3$ implants of the aragonite type when implanted subcutaneously in rats. No cells were involved in the production of this layer. Since the dissolution rate seems to be higher in a soft tissue environment the theory of dissolution and reprecipitation accounts for the establishment of the surface layer, which is similar to the pores in the present investigation.

The degradation of the $CaCO_3$ implants was either by dissolution or by cellular activity, i.e. by the action of osteoclast-like cells. Pits, large flat erosions, and tracks in the $CaCO_3$ surface were detected. For several years it has been known that osteoclasts can resorb $CaCO_3$. *In vitro*, isolated chick osteoclasts resorbed parts of calcite crystals, another crystal form of $CaCO_3$. These crystals had a face length of 30 μm which was chosen to avoid phagocytosis of single crystals [32]. The cells were of similar morphology to the cells in the present investigation and produced comparable pits. In the present study, two different types of resorbing cells were detected in contact with the implants. There were roundish cells with diameters of about 10 μm which produced the pits. Additionally, larger cells with an irregular structure of the outer cellular membrane due to pseudopods were observed in contact with large erosions of the implant surface. These observations are in accordance with other publications [8, 12, 33]. Therefore, different cell types are responsible for different types of resorption.

5. Conclusions

Natural coral implants induce woven bone formation on their surfaces, and formation of a distinct afibrillar intervening layer or cement-line like structure was not observed as is the case with lamellar bone deposition or bone bonding to stabile solid implant surfaces. Therefore, the mechanism leading to bone implant bonding in the case of degradable materials described herein needs subtle consideration of the current concept. The fast degradation of the material leads to an increased surface rugosity. The rough surface is colonized by flattened cells producing globular accretions on the tips of the implant surface. Due to the further degradation of the implant surface no morphologically distinct afibrillar intervening layer could develop. Therefore, collagen fibres produced by further differentiated cells insert on and between the tips of the implant surface providing contact to the implant and to the calcified globules. Thus, the implant surface was stabilized by bone bonding and no further degradation occurred in these areas. The further growth of the calcified globules and the further collagen production lead to the establishment of calcified fronts. The mineralization of the collagen-rich ECM is supported by matrix vesicles and by cell detritus which also acts in some cases as a calciumphosphate-crystal inducer. Therefore, an established stabile surface is a prerequisite for the development of the so-called afibrillar amorphous intervening layer. A second process leading to mineralized material was observed within the micropores. This process was dissolution dependent leading to reprecipitation, probably involving the adsorption of protein and P prior to the precipitation as demonstrated in an earlier publication [30]. The mineralization was coupled with resorption by multinuclear giant cells, probably osteoclasts, and by a smaller cell type. Additionally, dissolution led to decreasing particle size and particulate degradation in non-bone covered areas.

Acknowledgements

The study was supported by Inoteb, Paris, France. The authors are grateful to Mrs M. Dilger-Rhein for her excellent technical assistance.

References

1. R. T. CHIROFF, R. A. WHITE, E. W. WHITE, J. N. WEBER and D. ROY, *J. Biomed. Mater. Res.* **11** (1977) 165.
2. R. E. HOLMES, *Plast. Reconstr. Surg.* **63** (1979) 626.
3. G. GUILLEMIN, J.-L. PATAT, J. FOURNIE and M. CHETAIL, *J. Biomed. Mater. Res.* **21** (1987) 557.
4. G. GUILLEMIN, A. MEUNIER, P. DALLANT, P. CHRISTEL, J.-C. POULIQUEN and L. SEDEL, *ibid.* **23** (1989) 765.
5. M. ROUDIER, C. BOUCHON, J. L. ROUVILLAIN, J. AMÉDÉE, R. BAREILLE, F. ROUAIS, J. C. FRICAIN, B. DUPUY, P. KIEN, R. JEANDOT and B. BASSE-CATHALINAT, *ibid.*, **29** (1995) 909.

6. J. P. OUHAYOUN, A. H. M SHABANA, S. ISSAHAKIAN, J. L. PATAT, G. GUILLEMIN, M. H. SAWAF and N. FOREST, *J. Mater. Sci. Mater. Med.* **3** (1992) 222.
7. C. VOIGT, C. MERLE, C. MÜLLER-MAI and U. GROSS, *ibid.* **5** (1994) 688.
8. C. MÜLLER-MAI, C. VOIGT and U. GROSS, *Scanning Microsc.* **4** (1990) 613.
9. M. NEO, S. KOTANI, Y. FUJITA, T. NAKAMURA, T.YAMAMURO, Y. BANDO, C. OHTSUKI and T. KOKUBO, *J. Biomed. Mater. Res.* **26** (1992) 255.
10. U. M. GROSS, C. MÜLLER-MAI and C. VOIGT, in "The bone–biomaterial interface", edited by J. E. Davies (University of Toronto Press, Toronto, 1991) p. 308.
11. J. ZHANG, X. ZHANG, C. MÜLLER-MAI and U. GROSS, *J. Mater. Sci. Mater. Med.* **5** (1994) 243.
12. C. MÜLLER-MAI, S. I. STUBB, C. VOIGT and U. GROSS, *J. Biomed. Mater. Res.* **29** (1995) 9.
13. C. M. MÜLLER-MAI, C. VOIGT, R. E. BAIER and U. GROSS, *Cells and Materials* **2** (1992) 309.
14. U. GROSS, C. VOIGT and C. MÜLLER-MAI, *Bulletin de l'Institut Océanographique, numéro spécial* **14, 3** (1995) 85.
15. M. NEO, T. NAKAMURA, C. OHTSUKI, T. KOKUBO and T. YAMAMURO, *J. Biomed. Mater. Res.* **27** (1993) 999.
16. C. F. VOIGT, P. PELJAK, C. MÜLLER-MAI, H. HERBST, U. GROSS and G. FUHRMANN, *J. Mater. Sci. Mater. Med.* **6** (1995) 279.
17. G. GUILLEMIN and J. L. PATAT, in "Actualités en Biomatériaux", Vol. 1 (Editions Romillat, Paris, 1990) p. 151.
18. C. GENOVESE, D. ROWE and B. KREAM, *Biochemistry* **23** (1984) 6210.
19. S. MILANI, H. HERBST, D. SCHUPPAN, E. G. HAHN and H. STEIN, *Hepatology* **10** (1989) 84.
20. H. HERBST, E. STEINBRECHER, G. NIEDOBITEK, L. S. YOUNG, L. BROOKS, N. MÜLLER-LANTZSCH and H. STEIN, *Blood* **80** (1992) 484.
21. J. L. CORDELL, B. FALINI, W. N. ERBER, A. K. GHOSH, Z. ABDULAZIZ, S. MACDONALD, K. A. F. PULFORD, H. STEIN and D. Y. MASON, *J. Histochem. Cytochem.* **32** (1984) 219.
22. T. KOKUBO, S. ITO, Z. T. HUANG, T. HAYASHI, S. SAKKA, T. KITSUGI and T. YAMAMURO, *J. Biomed. Mater. Res.* **24** (1990) 331.
23. J. E. DAVIES, B. LOWENBERG and A. SHIGA, *ibid.* **24** (1990) 1289.
24. T. ALBREKTSSON, in "CRC critical reviews in biocompatibility", Vol. 1, Issue 1 (CRC Press Inc., Boca Raton, FL, 1984) p. 53.
25. G. GUILLEMIN, M. LAUNAY and A. MEUNIER, *J. Mater. Sci. Mater. Med.* **4** (1993) 575.
26. R. S. ARCHER, S. DOWNES, M. V. KAYSER and S. Y. ALI, *Cells and Materials* **2** (1992) 113.
27. J. D. DE BRUIJN, C. A. VAN BLITTERSWIJK and J. E. DAVIES, *J. Biomed. Mater. Res.* **29** (1995) 89.
28. H. ZHOU, R. CHERNECKY and J. E. DAVIES, *J. Bone Mineral Res.* **9** (1994) 367.
29. Y. FUJITA, T. YAMAMURO, T. NAKAMURA, S. KOTANI, C. OHTSUKI and T. KOKUBO, *J. Biomed. Mater. Res.* **25** (1991) 991.
30. H. KAWAGUCHI, M. D. MCKEE, H. OKAMOTO and A. NANCI, *Cells and Materials* **3** (1993) 337.
31. C. J. DAMIEN, J. L. RICCI, P. CHRISTEL, H. ALEXANDER and J. L. PATAT, *Calcif. Tissue* **55** (1994) 151.
32. S. J. JONES, A. BOYDE and N. N. ALI, *Scanning Electron Microscopy* **IV** (1986) 1555.
33. K. GOMI, J. D. DE BRUIJN, M. OGURA and J. E. DAVIES, *Cells and Materials* **3** (1993) 151.

Received 27 February
and accepted 22 December 1995